J. Plasma Physics (2006), *vol.* 72, *part* 3, *pp.* 309–327.
doi:10.1017/S0022377805004150 First published online 16 November 2005 Printed in the United Kingdom

The computation of field-line resonance frequencies in general geometries: a tool for improving the understanding of magnetospheric configurations

S. H. BEKHOR†

Department of Physics, University of Alberta, Edmonton, Alberta, Canada
(chalutz@umich.edu)

(Received 27 April 2005 and accepted 1 August 2005)

Abstract. Until recently, the calculation of field-line resonance (FLR) frequencies from magnetic field data, generated by magnetospheric models such as BATSRUS and Tsyganenko (T01), was restricted to orthogonal coordinate systems. With this restriction, only dipolar and axisymmetric configurations are admissible. The matter of addressing more general configurations such as non-axisymmetric stretched and twisted magnetic field topologies requires the use of a non-orthogonal coordinate system. This coordinate system can be constrained by defining the magnetic field as the product of Euler potentials, $\mathbf{B} = \nabla\alpha_i \times \nabla\alpha_j$, and imposing the condition, $\nabla \cdot \mathbf{B} = 0$, everywhere. As a consequence, the coordinates, α_i, must satisfy the partial differential equation, $\mathbf{B}\cdot\nabla\alpha_i = 0$. In other words, α_i must be constant along magnetic field lines. Upon solving this differential equation implicitly using known magnetic field intensities, the metric tensor for the resulting basis can be computed. The elements of this tensor can be substituted directly into the eigenvalue problem for general coordinate systems written in covariant notation. The equation for FLR modes has been developed for arbitrary incompressible magnetospheric conditions and has been specialized to the case where spatial variations are constrained along the magnetic field. The result is a fourth-order system of ordinary differential equations, which can be evaluated numerically, provided that the variation of the metric coefficients as a function of the distance along field lines is sufficiently smooth. The eigenvalue problem is solved at several latitudes for a broad range of magnetospheric conditions.

1. Introduction

Observations of low-frequency, nearly monochromatic shear Alfvén waves (SAW) are abundant in the Earth's magnetosphere. Of particular interest to both observers and theorists are anomalously low field-line resonance (FLR) frequencies between 1 and 3 mHz, which have been recorded near the midnight sector of the magnetosphere at latitudes corresponding to dipolar L-shells between 5 and 7. These low frequencies have sometimes been attributed to the stretching of magnetic

† Present address: Michigan Plasma Physics Research Institute, 1 Wood Avenue Suite 2002, Westmount, Québec, Canada, H3Z 3C5.

field lines relative to the dipolar topology (Warner and Orr 1979; Walker et al. 1992; Rankin et al. 2000), localized regions of elevated plasma density (Rankin et al. 1999; Strelsov and Lotko 1999) and to mode coupling with magnetosonic waves (Bhattacharjee et al. 1999). At present, there is no conclusive assessment that establishes any of these as the dominant factor responsible for the anomalous frequencies or whether these observations can be attributed to an external source such as the broadband fluctuation spectrum of the solar wind (De Keyser 2000).

This is a problem of considerable interest in magnetospheric physics as SAWs excited by FLRs can accelerate electrons in parallel electric fields. Both observation (Lui and Murphree 1998; Lotko et al. 1998) and simulation (Strelsov and Lotko 1999) suggest that this effect may be associated with discrete auroral arcs. In particular, FLR formation can lead to the structuring and narrowing of SAW resonances as well as the formation of density cavities. Thus, a thorough and formal description of the FLR drivers involved in these processes whereby energy flows from magnetohydrodynamic (MHD) waves to the resonant flux surface is essential.

The analytic characterization of ultra-low-frequency (ULF) waves in the Earth's magnetosphere depends strongly upon the model of the plasma dynamics used to describe the ambient medium, on the one hand, and upon the coordinate system used to approximate the global magnetic geometry. The model of choice for describing magnetospheric SAWs is the linearized single-fluid MHD set of equations. In the absence of strong coupling to fast and slow magnetosonic modes, an incompressible treatment is often used to compute the frequencies of the standing toroidal and poloidal modes.

On the other hand, the geometry used in order to solve this set of equations must be prescribed either by making simplifying assumptions about the ambient magnetic topology or by numerically constructing a coordinate system which conforms naturally to the magnetic field. In either case, the chosen geometry is specified by its corresponding metric tensor. Until recently, orthogonal magnetic-field-aligned coordinates, either dipolar or purely meridional, were used extensively to investigate ultra-low-frequency Alfvén wave resonances in the Earth's and other planetary magnetospheres (Cummings et al. 1969; Singer et al. 1981; Klimushkin et al. 1995; Rankin et al. 2000; Glassmeier et al. 2003). This approach, which permits the MHD equations to be written in generalized curvilinear coordinates, merits serious reconsideration as orthogonal coordinate systems can only be constructed in such a manner that they are properly oriented or aligned with the field lines in the absence of shear (Salat and Tataronis 2000).

Geomagnetic flux coordinates (GFC) were first critically discussed by Stern (1970) and more recently by D'haeseleer et al. (1991), and can be conveniently defined using the Euler or Clebsch representation. Upon being constructed, the intersections of the level surfaces defined by two of the coordinates, one that is radial-like and a generalized azimuthal coordinate, correspond to the field-line trajectories. These coordinates define the plane orthogonal to the magnetic field. A third field-aligned coordinate completes the coordinate triplet. To date, the full set of fully compressible linearized MHD equations have been solved for the dipolar magnetic topology (Proehl et al. 2002) and in more realistic quiet and disturbed time magnetospheres (Cheng and Zaharia 2002) using GFC. However, a direct comparison with orthogonal coordinate systems has yet to be presented. The primary objectives of this study are to quantify and characterize the error committed by using various orthogonal coordinate systems in the computation of field-line resonances in general

non-axisymmetric magnetospheric configurations and to determine to what degree the stretching of magnetic field lines at relatively low geographic latitude can, indeed, account for anomalously low observed FLR frequencies.

2. Curvilinear and more general coordinate systems

In this work, the advantage of using geomagnetic flux coordinates in comparison with commonly used orthogonal coordinate systems for the purpose of computing field-line resonance eigenmodes is investigated. Under certain magnetospheric conditions, in particular in the day sector and during extremely quiescent periods of solar activity, orthogonal coordinates may be used without committing significant errors. In the following sections, the magnitude of the error associated with using various orthogonal coordinate systems as magnetic field topologies become progressively stretched and twisted is quantified. Coordinate systems, in general, are characterized by their metric tensor. When an orthogonal coordinate system is used, the metric tensor is diagonal and generalized equations written in covariant notation simplify tremendously.

2.1. Orthogonal coordinate systems

The familiar orthogonal coordinate systems (α, β, μ) that are analyzed in this paper are the dipolar, purely meridional and grad B geometries. They are defined in the following manner.

Familiar dipolar coordinates

$$\alpha = \sin^2\theta/r, \tag{2.1}$$

$$\beta = \phi, \tag{2.2}$$

$$\mu = \cos\theta/r^2, \tag{2.3}$$

where θ, ϕ and r are the geomagnetic latitude and longitude and geocentric radius, respectively.

Purely meridional coordinates

$$\alpha = \sin^2\theta/r, \tag{2.4}$$

$$h_\beta = g_{\beta\beta}^{1/2} = (B_0 h_\alpha)^{-1}, \tag{2.5}$$

$$\mu \propto \text{distance along the magnetic field line from a point of reference}, \tag{2.6}$$

where h and g are the scale factors and metric coefficients corresponding to a particular coordinate, denoted by the subscripts, respectively, and B_0 is the ambient magnetic field intensity.

Grad *B* coordinates

Unit basis vectors are chosen in the $\mathbf{B}$, $\nabla|\mathbf{B}|$ and $\mathbf{B} \times \nabla|\mathbf{B}|$ directions.

Each of these coordinate systems is applicable to a particular magnetic geometry. As magnetic geometries become more realistic and depart from the above analytic expressions, calculations involving FLR eigenmodes progressively fail to capture the physics on a resonant surface. In differential geometry, this particular problem

https://doi.org/10.1017/S0022377805004150 Published online by Cambridge University Press

motivates the use of geodesics in order to map curved surfaces into geometries where they appear flat. Similarly, the use of GFC serves to examine the physics of ULF waves, in particular SAWs and slow magnetosonic waves, which exhibit magnetic guidance (Proehl and Lotko 2002), as oscillations in a straightened reference frame.

2.2. *Geomagnetic flux coordinates*

Geomagnetic flux coordinates (α, β, μ) must satisfy the following conditions:

$$\mathbf{B} = f(\alpha, \beta)[\nabla\alpha \times \nabla\beta] \tag{2.7}$$

$$\mu \propto \text{distance along the magnetic field line from a point of reference,} \tag{2.8}$$

where f (α, β) is a scalar function. Equation (2.7) implies the following necessary conditions for the Euler or Clebsch potentials α and β:

$$\mathbf{B} \cdot \nabla\alpha = 0 \tag{2.9}$$

$$\mathbf{B} \cdot \nabla\beta = 0. \tag{2.10}$$

In particular, (2.9) and (2.10) suggest that surfaces of constant α and β are tangential to the magnetic field at all points. Matched potentials satisfying (2.7) are not unique. In other words, several families of coordinate triplets satisfying the conditions for geomagnetic flux coordinates exist. In addition, there are a number of convenient ways to construct these triplets. For the problem at hand, we use the following boundary-constrained method to construct metric tensors for geomagnetic flux coordinates.

Scalar fields defined on some reference surface are chosen to be constant along magnetic field lines. Since the scalar potentials are matched at the reference surface, it follows that they are matched globally. The Earth's surface is a convenient choice for a reference surface because the magnetic field near the Earth's surface can be closely approximated by a dipole field. In this case, the potentials α and β are the familiar dipolar coordinates expressed in (2.1) and (2.2).

The Tsyganenko (T01) magnetospheric model uses the International Geomagnetic Reference Field (IGRF) Model in order to approximate the Earth's internal geomagnetic field. This multi-polar representation deviates by a few per cent from a dipole field at high latitudes. Nonetheless, α and β are very well matched up to a constant near the Earth's surface within a small neighborhood about each magnetic field line. In other words, $f(\alpha, \beta) \approx$ constant within a small flux tube surrounding each field line. For the sake of simplicity, the coefficient, $f(\alpha, \beta)$, is incorporated into the definitions of α and β in this paper. Once the Euler potentials prescribed on the ionospheric boundary surface are defined on a numerical grid superimposed onto the magnetosphere, the derivatives, $\nabla\alpha$ and $\nabla\beta$, can readily be computed in Cartesian coordinates using centered finite differences and a general field-line tracer. From these derivatives and the components of the magnetic field, $\mathbf{B}$, the inverse or dual of the desired symmetric metric tensor, g_{ij}, can be computed:

$$g^{ij} = \frac{\partial\alpha_i}{\partial x}\frac{\partial\alpha_j}{\partial x} + \frac{\partial\alpha_i}{\partial y}\frac{\partial\alpha_j}{\partial y} + \frac{\partial\alpha_i}{\partial z}\frac{\partial\alpha_j}{\partial z}, \tag{2.11}$$

where $\boldsymbol{\alpha} \equiv [\alpha, \beta, \mu]$. The partial derivatives in (2.11) are none other than the components of $\nabla\alpha, \nabla\beta$ and $\mathbf{B}$ in Cartesian coordinates. The metric tensor, g_{ij}, specifies the basis and contains the coefficients necessary to solve the incompressible and compressible MHD equations in GFC.

https://doi.org/10.1017/S0022377805004150 Published online by Cambridge University Press

3. The FLR eigenmode equations

The equations for FLR modes are developed for arbitrary incompressible magnetospheric conditions. They follow immediately from Maxwell's equations in MKS units once knowledge of the rationalized dielectric tensor, A^{if}, is invoked:

$$\frac{1}{\sqrt{g}}\left(\frac{\partial E_k}{\partial x^j}-\frac{\partial E_j}{\partial x^k}\right)=-\frac{\partial B^i}{\partial t} \tag{3.1}$$

$$\frac{1}{\sqrt{g}}\left(\frac{\partial H_k}{\partial x^j}-\frac{\partial H_j}{\partial x^k}\right)=\frac{\partial D^i}{\partial t}+J^i=\varepsilon_0 A^{if}\frac{\partial E_f}{\partial t}+J^i_{\text{ext}}, \tag{3.2}$$

where

$$A^i_f=-\frac{g_{jf}}{\sqrt{g}}\varepsilon^{j\mu k}\frac{v_{\text{A}\mu}\sqrt{g}_{\mu\mu}}{c}\frac{g_{jk}}{\sqrt{g}}\varepsilon^{j\mu i}\frac{v_{\text{A}\mu}\sqrt{g}_{\mu\mu}}{c} \tag{3.3}$$

$$v_{\text{A}\mu}=\frac{B_{0\mu}}{\sqrt{\mu_0\rho_0}}, \tag{3.4}$$

where $v_{\text{A}\mu}$ is the local Alfvén speed, $B_{0\mu}$ is the ambient magnetic field intensity, μ_0 is the permeability of free space, ε_0 is the permittivity of free space, ρ_0 is the mass density and c is the speed of light in a vacuum. In the above equations, g is the determinant of the metric tensor, g_{ij}. E_i, D_i, H_i, B_i, J_i and $J_{\text{ext},i}$ are the components of the electric field, electric displacement field, magnetic field intensity, magnetic flux density, current density and background current density, respectively. As mentioned in the previous section, one of the coordinates, μ, is also assumed to be aligned with the ambient magnetic field without any loss of generality.

The dielectric tensor in the above system of equations is evaluated using the frozen-in generalized Ohm's law with infinite conductivity and the momentum equation, where the background plasma ring current and hot plasma gradients are ignored. The background current appears on the right-hand side of (3.2) and is neglected in this calculation. These approximations are justified for most magnetospheric plasmas (Singer et al. 1981). A comparison of the fully compressible MHD equations in different coordinate systems is reserved for future work.

Solutions to this set of equations are assumed to have temporal variations of the form, $e^{i\omega t}$. The result is a set of partial differential equations in terms of the spatial variables, x_i. Equations (3.1) and (3.2) can be rewritten conveniently and compactly using the cyclic permutation matrix, ε^{ijk}:

$$-i\omega\sqrt{g}B^i=\varepsilon^{ijk}\partial_j E_k \tag{3.5}$$

$$i\omega\sqrt{g}c^2A^{if}E_f=\varepsilon^{ijk}\partial_j B_k, \tag{3.6}$$

where

$$\partial_i\equiv\frac{\partial}{\partial x^i}. \tag{3.7}$$

The resulting eigenmode equation follows upon lowering the indices on the left-hand sides of (3.5) and (3.6) and inverting the dielectric tensor:

$$\frac{g_{ij}}{\sqrt{g}}\varepsilon^{ilf}\partial_l\left(c^2A^k_f\frac{g_{ik}}{\sqrt{g}}\varepsilon^{imk}\partial_m B_k\right)=\omega^2B_j. \tag{3.8}$$

https://doi.org/10.1017/S0022377805004150 Published online by Cambridge University Press

For the purpose of this study, it is useful to examine the above equation in a limit that is relevant to most magnetospheric plasmas. It is often reasonable to assume that spatial variations are constrained primarily along the magnetic field lines, i.e. (along μ). In this limit, (3.8) has the following convenient representation:

$$\omega^2 B_\varkappa = \gamma_{1\varkappa}\partial_\mu f_\varkappa + \gamma_{2\varkappa} f_\varkappa + \gamma_{3\varkappa} f_\beta \tag{3.9}$$

$$\omega^2 B_\beta = \gamma_{1\beta}\partial_\mu f_\beta + \gamma_{2\beta} f_\beta + \gamma_{3\beta} f_\varkappa, \tag{3.10}$$

where $f_\varkappa = \partial_\mu B_\varkappa$, $f_\beta = \partial_\mu B_\beta$,

$$\gamma_{1\alpha} = \gamma_{1\beta} = -v_{\mathrm{A}}^2 \frac{g_{\alpha\alpha}}{\sqrt{g}}\frac{g_{\beta\beta}}{\sqrt{g}} + v_{\mathrm{A}}^2 \frac{g_{\alpha\beta}}{\sqrt{g}}\frac{g_{\alpha\beta}}{\sqrt{g}}, \tag{3.11}$$

$$\gamma_{2\alpha} = -\frac{g_{\alpha\alpha}}{\sqrt{g}}\partial_\mu\left(v_{\mathrm{A}}^2 \frac{g_{\beta\beta}}{\sqrt{g}}\right) + \frac{g_{\alpha\beta}}{\sqrt{g}}\partial_\mu\left(v_{\mathrm{A}}^2 \frac{g_{\alpha\beta}}{\sqrt{g}}\right), \tag{3.12}$$

$$\gamma_{3\alpha} = \frac{g_{\alpha\alpha}}{\sqrt{g}}\partial_\mu\left(v_{\mathrm{A}}^2 \frac{g_{\alpha\beta}}{\sqrt{g}}\right) - \frac{g_{\alpha\beta}}{\sqrt{g}}\partial_\mu\left(v_{\mathrm{A}}^2 \frac{g_{\alpha\alpha}}{\sqrt{g}}\right), \tag{3.13}$$

$$\gamma_{2\beta} = -\frac{g_{\beta\beta}}{\sqrt{g}}\partial_\mu\left(v_{\mathrm{A}}^2 \frac{g_{\alpha\alpha}}{\sqrt{g}}\right) + \frac{g_{\alpha\beta}}{\sqrt{g}}\partial_\mu\left(v_{\mathrm{A}}^2 \frac{g_{\alpha\beta}}{\sqrt{g}}\right), \tag{3.14}$$

$$\gamma_{3\beta} = \frac{g_{\beta\beta}}{\sqrt{g}}\partial_\mu\left(v_{\mathrm{A}}^2 \frac{g_{\alpha\beta}}{\sqrt{g}}\right) - \frac{g_{\alpha\beta}}{\sqrt{g}}\partial_\mu\left(v_{\mathrm{A}}^2 \frac{g_{\beta\beta}}{\sqrt{g}}\right), \tag{3.15}$$

$$v_{\mathrm{A}}^2 = v_{\mathrm{A}\mu}^2 g_{\mu\mu}\left(\frac{g_{\alpha\alpha}g_{\beta\beta} - g_{\alpha\beta}g_{\alpha\beta}}{g}\right). \tag{3.16}$$

For the purpose of confirmation, it is worthwhile to observe that (3.8) reduces to the familiar uncoupled equations for the standing poloidal and toroidal shear Alfvén waves in dipolar coordinates. This information can be extracted from the equations for general orthogonal coordinates in which the metric tensor is diagonal ($g = g_{\varkappa\varkappa}g_{\beta\beta}g_{\mu\mu}$). In this case, only the first terms in $\gamma_{1\varkappa}$, $\gamma_{2\varkappa}$, $\gamma_{1\beta}$ and $\gamma_{2\beta}$ are retained:

$$-\omega^2 B_\alpha = \sqrt{\frac{g_{\alpha\alpha}}{g_{\beta\beta}}}\frac{1}{\sqrt{g_{\mu\mu}}}\partial_\mu\left(\sqrt{\frac{g_{\beta\beta}}{g_{\alpha\alpha}}}\frac{v_{\mathrm{A}\mu}^2 f_\alpha}{\sqrt{g_{\mu\mu}}}\right) \quad \text{(toroidal)} \tag{3.17}$$

$$-\omega^2 B_\beta = \sqrt{\frac{g_{\beta\beta}}{g_{\alpha\alpha}}}\frac{1}{\sqrt{g_{\mu\mu}}}\partial_\mu\left(\sqrt{\frac{g_{\alpha\alpha}}{g_{\beta\beta}}}\frac{v_{\mathrm{A}\mu}^2 f_\beta}{\sqrt{g_{\mu\mu}}}\right) \quad \text{(poloidal)}. \tag{3.18}$$

The sets of ordinary differential equations (ODEs) for both the diagonal and the non-diagonal metric tensors can be solved using a shooting method. One boundary condition is prescribed by ignoring the small, but finite ionospheric resistivity and assuming that the ionosphere is a perfect spherical conductor with the artificially large geocentric radius of $3R_{\mathrm{E}}$. Placement of the ionopause closer to the Earth's surface does not significantly alter the computed eigenfrequencies in this paper, most notably at high latitudes. However, at low latitudes, where an increase in FLR frequencies is both predicted and observed, the elevated mass densities in the immediate vicinity of the Earth's surface produce distortions in the computed eigenfunctions. In particular, wavelengths computed very close to the Earth tend to be much longer than those at higher altitude and especially near the equatorial

https://doi.org/10.1017/S0022377805004150 Published online by Cambridge University Press

crossing of a field line. When the magnetospheric density profile described in Sec. 4 is chosen, this problem can be avoided by prescribing the ionospheric boundary above $1.5R_E$. Perfectly conducting boundary conditions imply that the tangential electric field vanishes at the interface; hence, $f_{\alpha 0} = f_{\beta 0} = 0$.

In the diagonal case, the eigenmode equations are uncoupled and, therefore, the polarizations are either purely toroidal or purely poloidal. In the non-diagonal case, a two-dimensional root finder is used in order to determine the correct boundary conditions for B_α and for B_β or equivalently the correct polarization at the boundary interface, $\varphi = \tan^{-1}(B_{\beta 0}/B_{\alpha 0})$, as well as the correct eigenfrequency, ω.

4. Magnetospheric conditions

In this paper, a crude static model of the magnetospheric density profile is assumed for the purpose of calculating the Alfvén speed, $v_{A\mu}$. Though this model is a reasonable representation of the plasma density throughout much of the magnetosphere, it overvalues the density at low altitude, a region that has been purposefully excluded from these calculations. In addition, the model fails to account for the variable thickness of the plasmasphere, the region just above the ionosphere where the plasma density decays more slowly with geocentric radius, as a function of L-shell and the time of day. In this model, a two-species plasma is prescribed. Hydrogen ions are assumed to have a constant number density, n_H, of 1 cm^{-3}. The oxygen ion density is assumed to decrease exponentially with altitude, h, from a reference value, n_0, of 10^6 cm^{-3} at the Earth's surface with a characteristic length scale, h_0, of $0.1R_E$:

$$n_{\text{eff}} = n_H + m_0 n_0 \exp(-h/h_0)$$

$$m_0 = 16 \text{ (oxygen mass in amu)}$$

$$v_{A\mu}^2 = |B|^2/(\mu_0 m_H n_{\text{eff}})$$

$$m_H = \text{proton mass.}$$

The oxygen component in the density does not seem to significantly affect this calculation. The cases that are reported in this paper correspond to magnetospheric conditions at 21h00 UT on December 16, 1995, a date close to the solar minimum. The solar wind pressure is set to 3 nPa. The disturbance storm time (DST) index is set to −20 nT and two components of the interplanetary magnetic field are set to $B_y = 0$ and $B_z = 10$ nT. The geographic longitude of field lines under consideration is 45°. The latitude varies from 45° to 62.2° at an altitude of $3R_E$.

5. Results and discussion

The frequencies and polarizations at the northern hemispheric boundaries for the fundamental quasi-toroidal (mode 1) and quasi-poloidal (mode 2) as well as the first four harmonic (modes 3–6) eigenmode solutions to (3.9) and (3.10) are depicted in Figs 2 and 3 as a function of the dipolar L-shell index referenced at 1 Earth radius in the northern hemisphere. The ordinates in these plots correspond to the discrete field lines whose equatorial, meridional and frontal projections are illustrated in Fig. 1. For the analog of the toroidal mode in dipolar coordinates, frequencies

https://doi.org/10.1017/S0022377805004150 Published online by Cambridge University Press

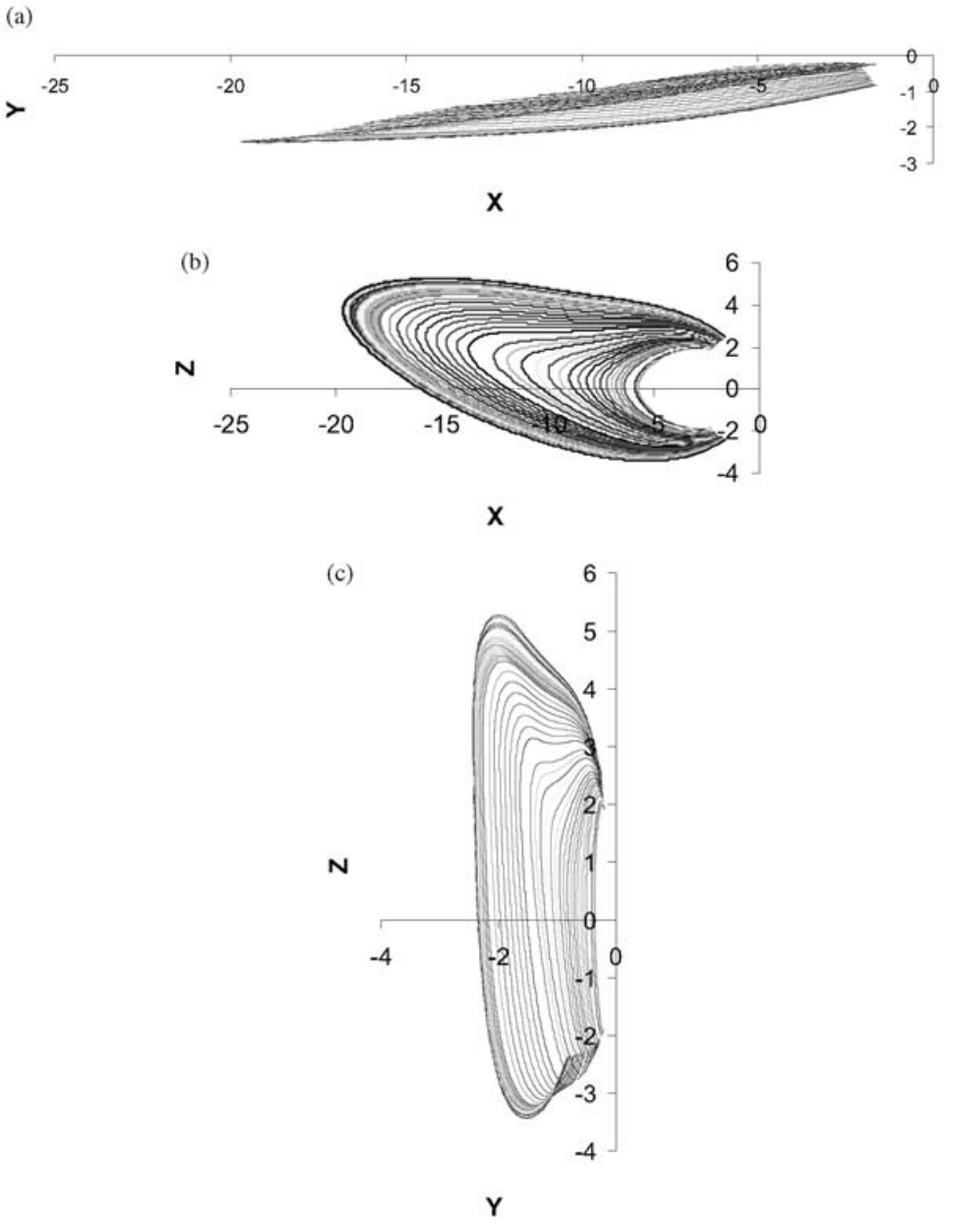

Figure 1. (a) Equatorial, (b) meridional and (c) frontal field-line projections from 45° to 62.2° latitude.

range from about 30 mHz at low latitude ($L = 4.5$) to 1.4 mHz at relatively high latitudes ($L = 8.6$) in conditions where magnetic field topologies are stretched and non-axisymmetric. In the case of the quasi-poloidal mode, frequencies range from about 50 mHz to about 2 mHz. Each of these modes has a distinct polarization at the boundary. For the quasi-toroidal mode, the polarization is fairly constant

https://doi.org/10.1017/S0022377805004150 Published online by Cambridge University Press

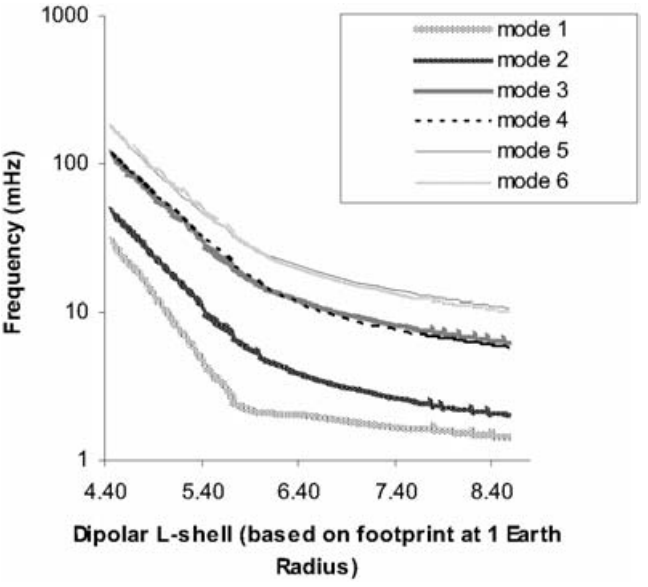

Figure 2. Six lowest field-line resonance eigenfrequencies in the non-dipolar, non-axisymmetric topology (GFC used).

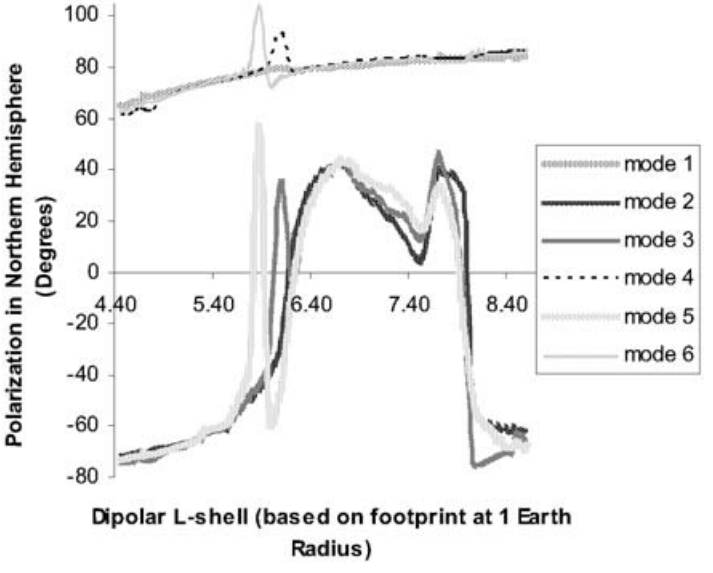

Figure 3. Polarizations of field lines at the northern hemispheric boundary (GFC used).

with increasing L-shell, whereas the polarization varies considerably for the quasi-poloidal mode.

These polarizations are reproduced to a good approximation for the harmonic modes, except when pairs of modes are frequency-matched. In this case, the coupling of two modes results in an observed shift in the polarizations. Frequency-matching occurs at different L-shells for the second and third harmonics, for which

https://doi.org/10.1017/S0022377805004150 Published online by Cambridge University Press

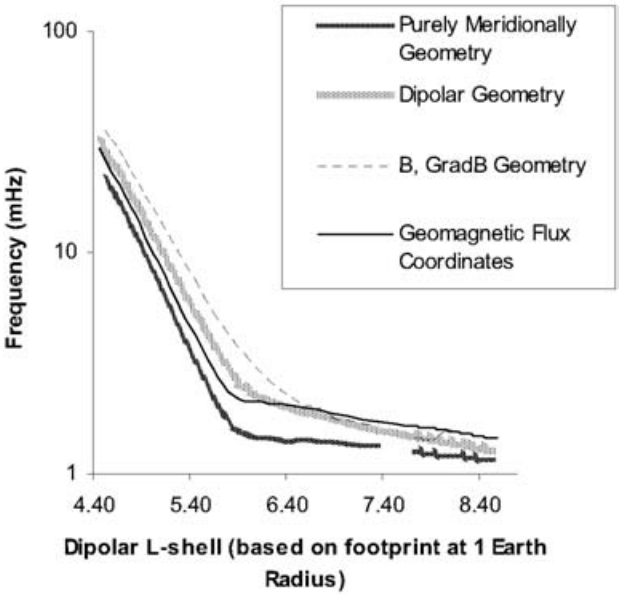

Figure 4. Lowest eigenmode in various coordinate systems (non-dipolar topology).

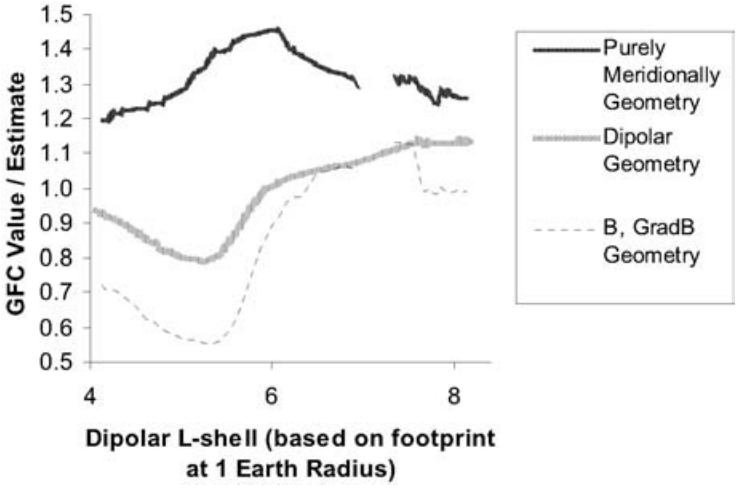

Figure 5. Discrepancy in the frequency of the lowest eigenmode in calculations where orthogonal coordinates are used.

the frequencies are relatively close over the entire range of L-shells under examination. For the first harmonics, matching occurs at an L-shell of about 6.6, whereas for the second harmonics it occurs at an L-shell of about 5.9. It should be noted, however, that in the presence of kinetic damping and finite ionospheric resistivity the computed resonances would be broadened and weakened. Therefore, it is likely that resonance occurs and that mode conversion is an important process over the entire range of L-shells. Mode conversion has frequently been used to explain localized resonant amplification of wave amplitudes, especially in regions

https://doi.org/10.1017/S0022377805004150 Published online by Cambridge University Press

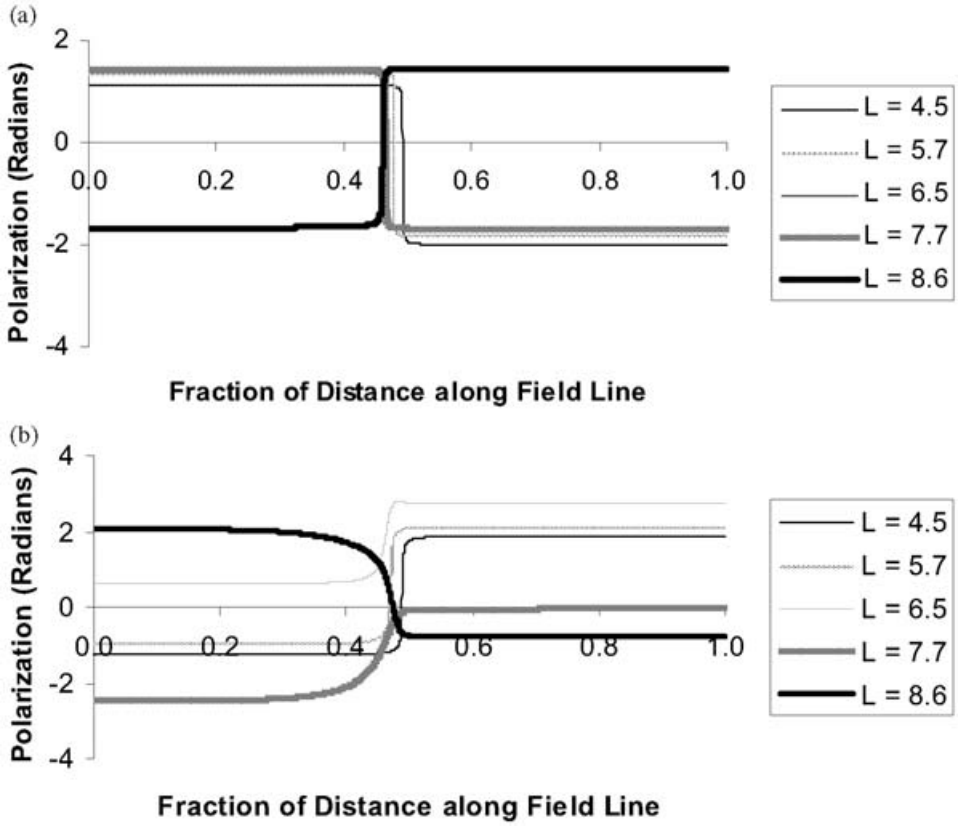

Figure 6. Polarizations of the four lowest Modes in the flux coordinate geometry along five representative field lines: (a) quasi-toroidal mode, (b) quasi-poloidal mode, (c) harmonic 1 and (d) harmonic 2.

of plasma inhomogeneity (De Keyser 2000). This is an important effect in the description of magnetic storm and sub-storm dynamics, the impact of which can be properly assessed in the crossed-phase analyses of related observations.

An informative comparison of orthogonal and non-orthogonal coordinate systems can be achieved by comparing the frequency of the quasi-toroidal eigenmode computed in the different geometries. Figures 4 and 5 clearly demonstrate the limitations of orthogonal geometries. In each case, the frequency is either overestimated or underestimated when field lines are deformed with respect to the dipolar topology. In particular, the purely meridional geometry (Singer et al. 1981) accounts for the elongation of field lines at high latitude, which tends to decrease the computed frequency (Rankin et al. 2000). However, it underestimates the resonant frequency along field lines that are sheared out of the meridional plane by almost one-third in the severely deformed topology corresponding to the dipolar L-shell of 6.5. The ratio of frequencies computed in GFCs and the purely meridional coordinate system can be used to determine to what extent the actual field-line topology deviates from the purely meridional topology. In other words, it is an indirect measure of field-line torsion.

https://doi.org/10.1017/S0022377805004150 Published online by Cambridge University Press

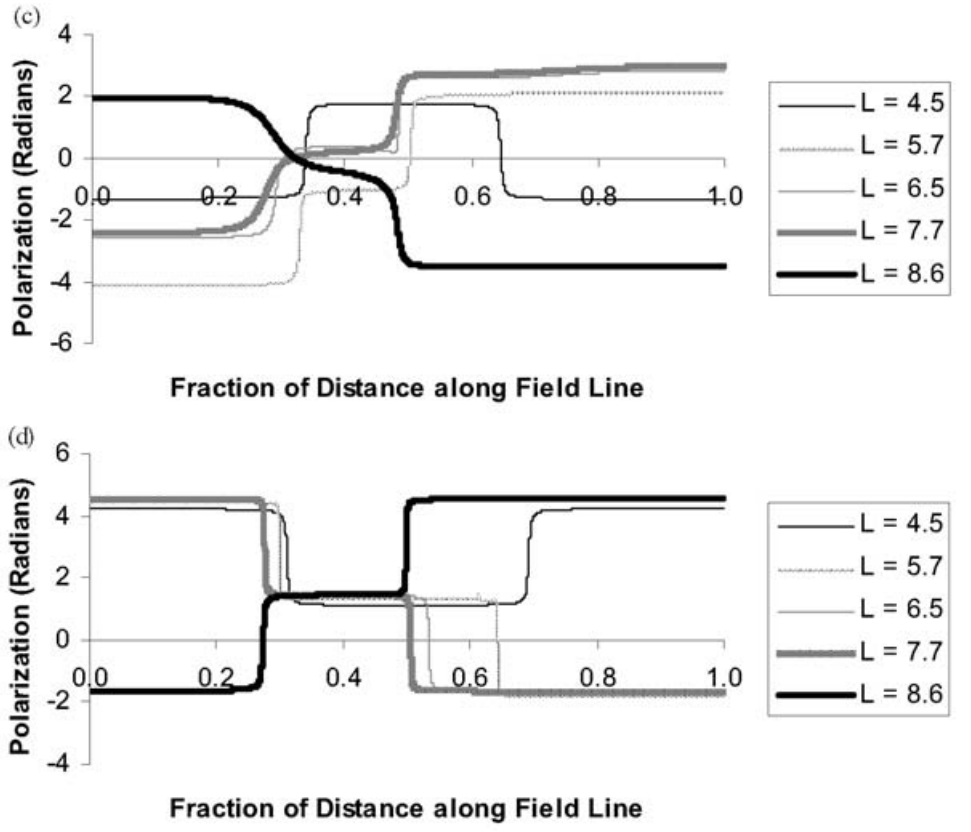

Figure 6. Continued.

The **B**, ∇B representation, discussed in Sec. 2.1, exaggerates the effect of field-line torsion, which tends to increase the computed frequencies. This is particularly apparent at low L-shells where field lines are barely stretched with respect to the dipolar topology; hence, eigenfrequencies are overestimated by a factor of as much as 1.8. It also exaggerates the effect of field-line stretching, which becomes pronounced at L-shells above 5.5. Conveniently, the two effects cancel one another at sufficiently high L-shell, where the eigenfrequency computed in grad-B coordinates very closely matches that computed in GFC. The best orthogonal geometry seems to be the dipolar representation which provides a good estimate of the fundamental frequency except when one type of field-line deformation is clearly dominant. Between L-shells of 4.5 and 6.3, torsion dominates, whereas stretching becomes dominant above L-shell values of 6.3. In this case, eigenfrequencies are slightly overestimated for the nearly dipolar low L-shell field lines and slightly underestimated for the stretched high L-shell field lines.

Figure 6 shows the polarizations of the four lowest eigenmodes in the flux coordinate geometry along five field lines (dipolar L-shells 4.5, 5.7, 6.5, 7.7 and 8.6). Among these, the field-lines at L-shells 7.7 and 8.6 are the most stretched relative to the dipolar topology and, as illustrated in Fig. 1, are the most asymmetric about the geomagnetic equator. Therefore, the eigenfunctions and polarizations of the resonant modes on these field lines are not expected to be symmetric. Evidence of

https://doi.org/10.1017/S0022377805004150 Published online by Cambridge University Press

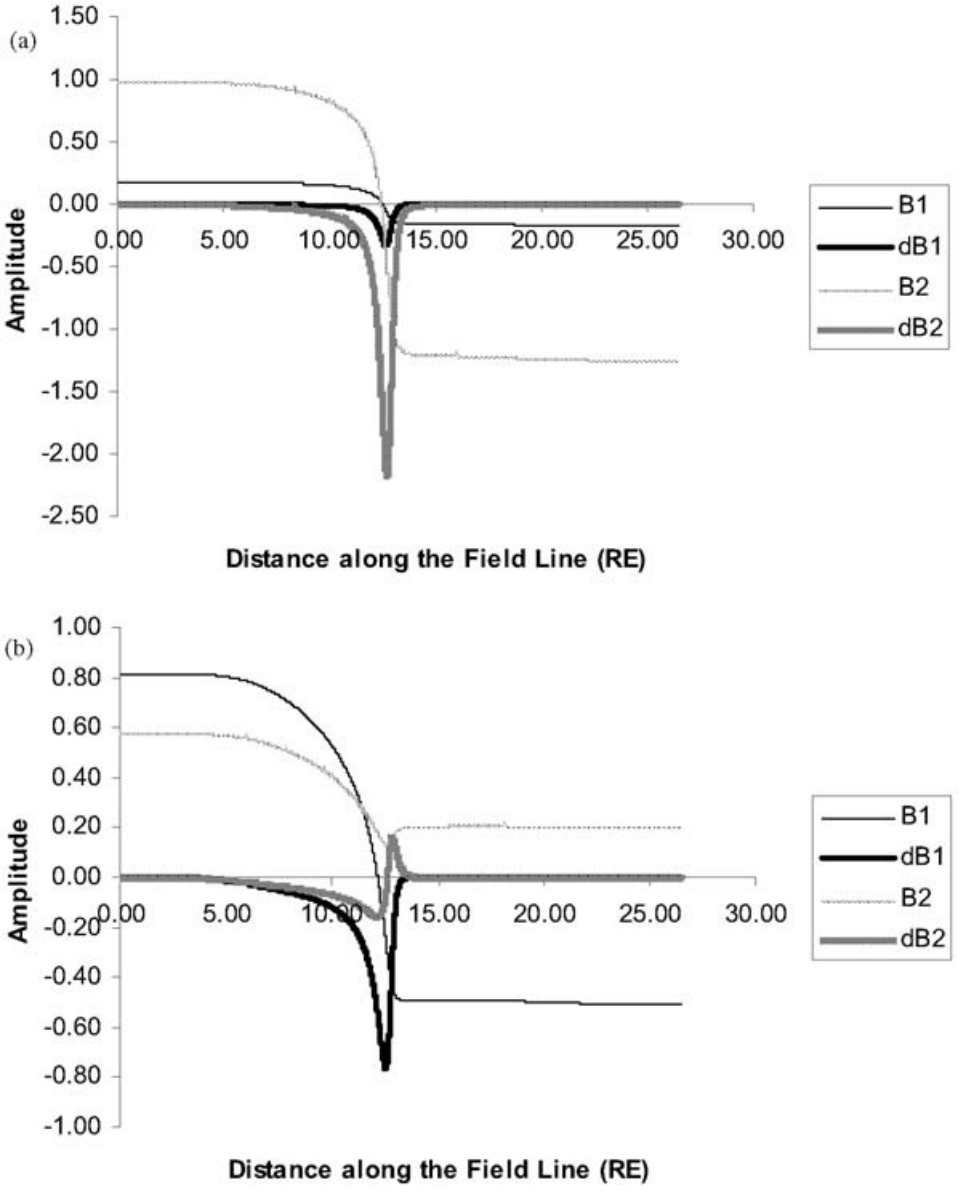

Figure 7. Eigenfunctions and their first derivatives of the four lowest eigenmodes along a stretched and twisted field line ($L = 6.5$) in geomagnetic flux coordinates: (a) quasi-toroidal mode, (b) quasi-poloidal mode, (c) harmonic 1 and (d) harmonic 2.

the latter manifests itself in the plots as a more gradual reversal of polarity near the equator for the antisymmetric fundamental modes. Furthermore, the reversals in polarization move progressively toward the left or toward the northern hemispheric boundary with increasing L-shell. In particular, the polarization of field lines exhibits a gradual departure from perfect symmetry with increased deformation in the case of the quasi-poloidal mode in Fig. 6(b). Though the departure from symmetry is less evident in the case of the quasi-toroidal mode in Fig. 6(a), it is nonetheless

https://doi.org/10.1017/S0022377805004150 Published online by Cambridge University Press

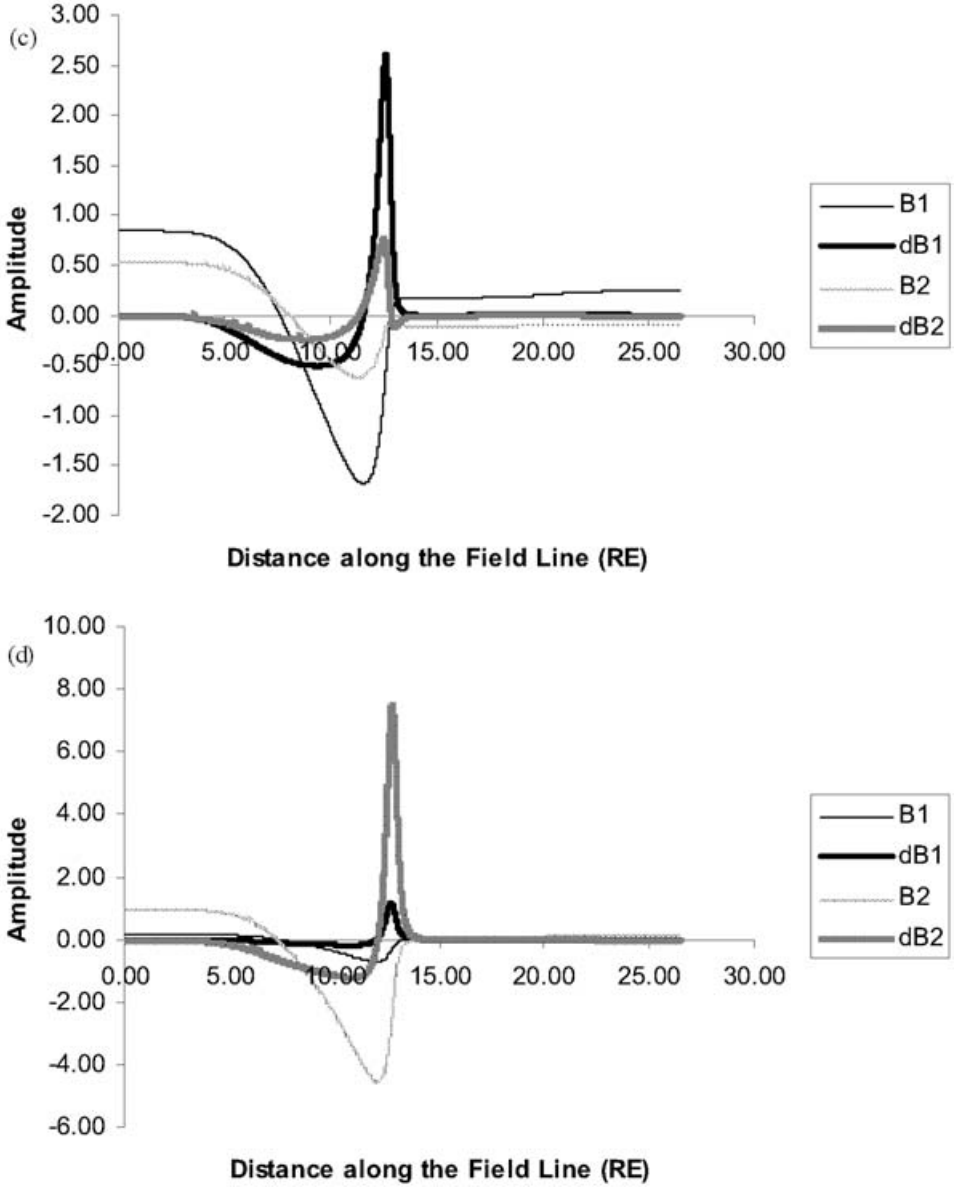

Figure 7. Continued.

present. The more gradual reversals in the northern and southern hemispheres and the loss of symmetry are also observed for the pseudo-symmetric harmonic modes, especially in Fig. 6(c).

Figure 7 shows the eigenfunctions of the four lowest modes for the most twisted field line ($L = 6.5$) and their first derivatives with respect to the field-aligned coordinate in the geomagnetic flux coordinate geometry. The effect of torsion has a direct consequence upon the character of the generalized azimuthal coordinate component, B_2, of the quasi-poloidal mode and its first harmonic. In particular,

https://doi.org/10.1017/S0022377805004150 Published online by Cambridge University Press

the plot of this component in Fig. 7(b) exhibits two changes in curvature. For the fundamental modes of field lines without torsion, only one change in curvature is expected. This property is also observed as a small hump near the equator in the polarization plot for $L = 6.5$ in Fig. 6(b). Similarly, the generalized azimuthal coordinate component in Fig. 7(c) exhibits three changes in curvature instead of two for one of the harmonics. In Fig. 6(c), this effect manifests itself as a small depression in the polarization plot half-way along the field line. This feature is not present in the four other field lines under examination.

The eigenfunctions can also be rendered in dipolar coordinates by using the following transformation:

$$u_k^{\mathrm{dip}} = g_{jk}^{\mathrm{dip}} g^{ij} u_i. \tag{5.1}$$

Figures 8 and 9 show the same eigenfunctions in Fig. 7 for the $L = 4.5$ and 6.5 field lines in dipolar coordinates. At low L-shell, only the effect of mild field-line torsion is apparent. The eigenfunctions exhibit the expected symmetries of dipole field lines to a large degree. However, the polarizations of the eigenmodes are no longer purely toroidal or purely poloidal. In the stretched and twisted topology, this resemblance disappears completely and the departure from symmetry becomes very apparent. In addition, for the $L = 6.5$ field line only, the unusual hump or depression near the equator for the quasi-poloidal mode and its first harmonic appears in both of the dipolar coordinates.

6. Conclusion

In the present work, the error due to approximating magnetic field geometries using orthogonal coordinate systems is quantified by making direct comparisons for a set of field lines in the near-midnight sector of the magnetosphere during a relatively quiescent period. In particular, the most commonly used orthogonal coordinate system, purely meridional coordinates, is demonstrated to underestimate the frequency of the toroidal mode in the presence of significant field-line torsion by as much as one-third. Two other orthogonal coordinate systems, dipolar and grad-B coordinates, overestimate the frequency in the presence of field-line torsion. Moreover, previous work that attempts to justify anomalously low observed FLR frequencies, especially in the sub-millihertz range, by invoking considerable stretching at relatively low latitudes corresponding to dipole L-shells between 6 and 7 is probably not comprehensive. More detailed models of the magnetospheric plasma density and mode coupling may be required to match theory with observations.

In order to perform the above analysis, boundary-constrained geomagnetic flux coordinates and a mixed covariant/contravariant formalism are used to compute FLR frequencies assuming spatially inhomogeneous, incompressible MHD. For the sake of simplicity, the boundary surface that is chosen to specify the flux surfaces in this problem is the Earth's surface, where magnetic field-line topologies approach dipolarity. In addition, the ionospheric boundary is assumed to be a perfectly conducting spherical shell and is placed at an artificially high geocentric altitude of $3R_{\mathrm{E}}$. In another study (Proehl et al. 2002), both the boundary surface used to prescribe GFCs and the ionopause are placed at $2R_{\mathrm{E}}$. By doing so, derivatives of the GFC with respect to the Cartesian basis can be calculated by using finite differences and the metric tensor prescribing the conformal magnetic geometry can be evaluated.

https://doi.org/10.1017/S0022377805004150 Published online by Cambridge University Press

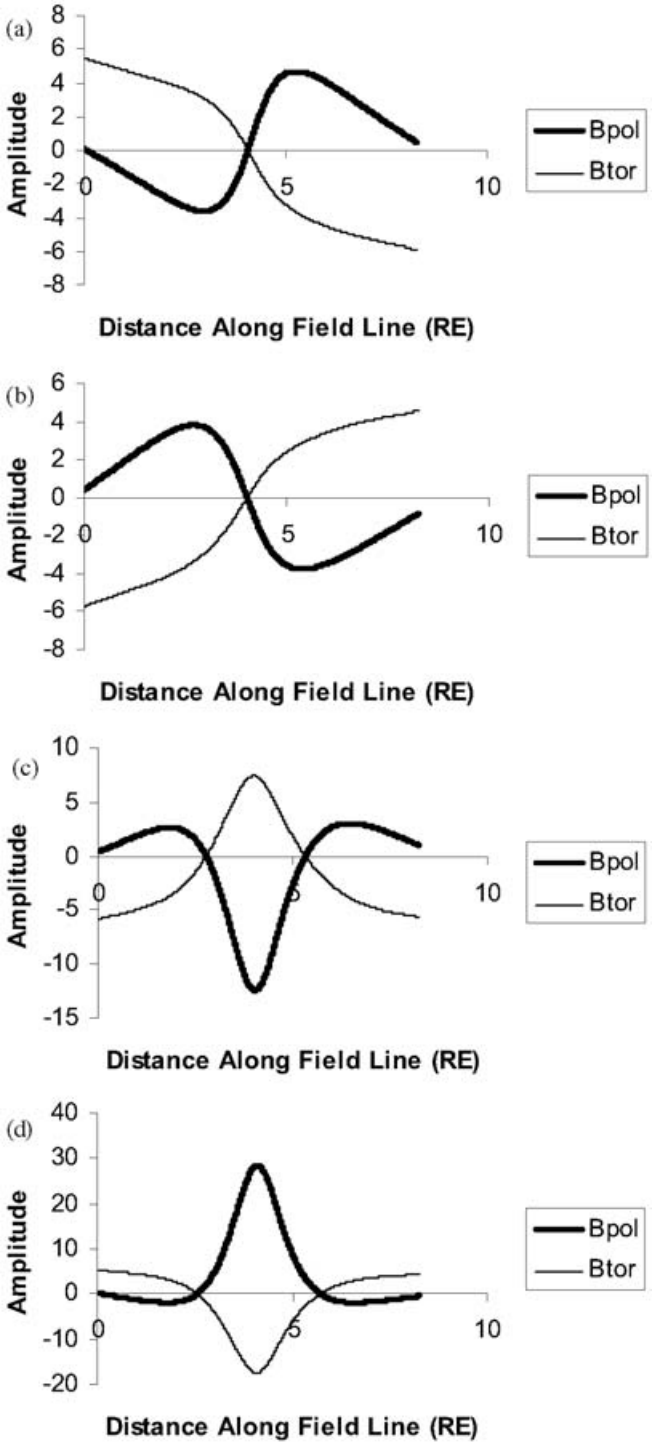

Figure 8. Eigenfunctions of the four lowest eigenmodes along a nearly dipolar (low $L = 4.5$ shell) field line upon converting to dipolar coordinates: (a) quasi-toroidal, (b) quasi-poloidal, (c) harmonic 1 and (d) harmonic 2.

https://doi.org/10.1017/S0022377805004150 Published online by Cambridge University Press

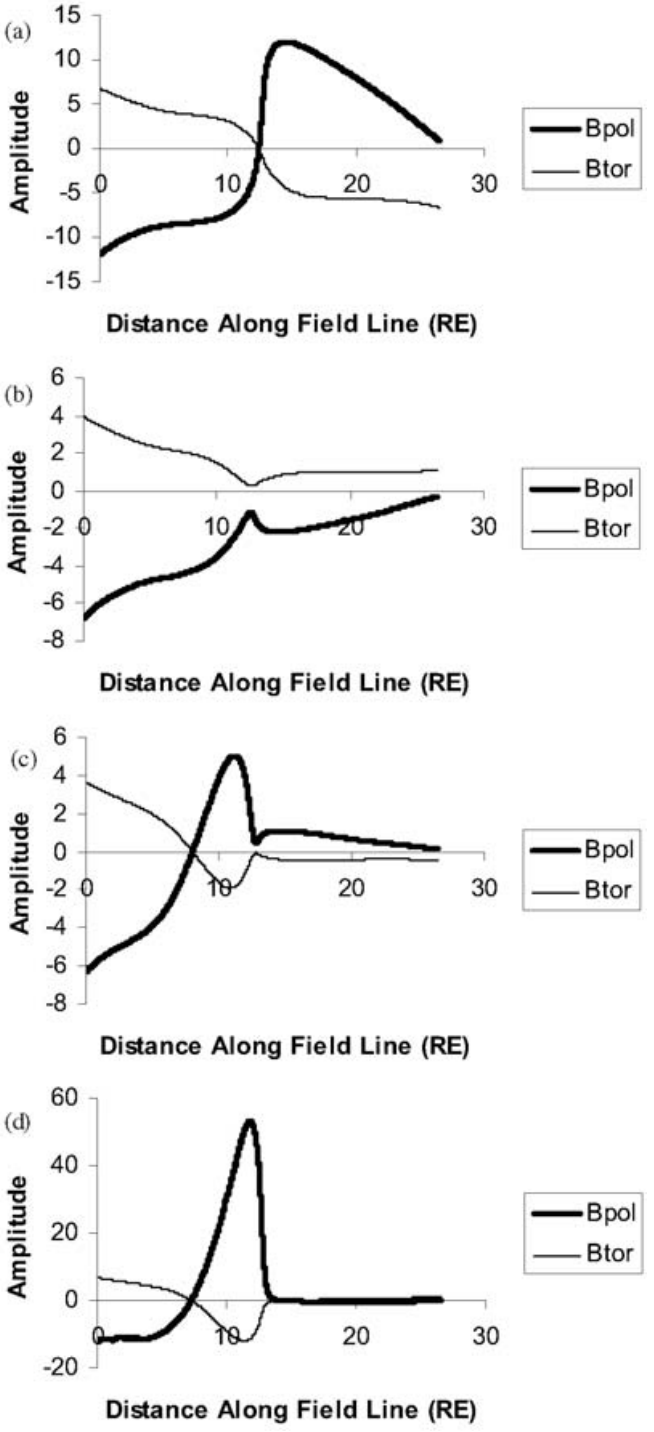

Figure 9. Eigenfunctions of the four lowest eigenmodes along a stretched and twisted field line ($L = 6.5$) upon converting to dipolar coordinates: (a) quasi-toroidal, (b) quasi-poloidal, (c) harmonic 1 and (d) harmonic 2.

https://doi.org/10.1017/S0022377805004150 Published online by Cambridge University Press

The approach advanced in this paper is especially relevant to crossed-phase analyses performed at times when there is a strong interaction between the solar wind and the Earth's magnetic field. The result of strong solar wind–magnetosphere coupling is the deformation of the magnetic field topology away from a nearly dipolar equilibrium, especially at high latitude. Therefore, high-latitude observations from ground-based arrays and spacecraft would strongly benefit from a more thorough comparison with both incompressible and compressible theories solved in geomagnetic flux coordinates.

In particular, crossed-phase analyses would be especially helpful in identifying the driving modes that excite discrete magnetospheric phenomena. These modes can be prescribed in order to study the linear and nonlinear evolution of dispersive FLRs. The subsequent structuring of FLRs and density steepening lead to the trapping of SAWs inside nonlinear density perturbations (Lu et al. 2003). An accurate FLR solver in conjunction with detailed observations can also assist in solving the inverse problem of dynamically mapping the density profile of the magnetosphere during magnetic storms and sub-storms (Waters 2000; Takahashi et al. 2004). Beyond the magnetosphere, the method described in this paper can be used to facilitate the study of resonant Alfvén wave heating in solar coronal loops (Berghmans and de Bruyne 1995; Ofman and Davila 1996).

Acknowledgement

I would like to acknowledge Richard Marchand of the University of Alberta for fruitful and constructive discussions and interactions that helped me in the production of this work.

References

Bhattacharjee, A., Kletzing, C. A., Ma, Z. W. Otani, N. F. and Wang, X. 1999 Four-field model for dispersive field line resonances: effects of coupling between shear-Alfvén and slow modes. *Geophys. Res. Lett.* **26**, 3281.

Berghmans, D. and de Bruyne, P. 1995 Coronal loop oscillations driven by footpoint motions: analytical results for a model problem. *Astrophys. J.* **453**, 495.

Cheng, C. Z. and Zaharia, S. 2002 Field line resonances in quiet and disturbed time three-dimensional magnetospheres. *J. Geophys. Res.* **100**, 9527–9534.

Cummings, W. D., O'Sullivan, R. J. and Coleman, P. J. Jr. 1969 Standing Alfvén waves in the magnetosphere. *J. Geophys. Res.* **74**, 778.

D'haeseleer, W. D. D., Hitchon, W. N. G., Callen, J. D. and Shohet, J. L. 1991 *Flux Coordinates and Magnetic Field Structure*. New York: Springer.

De Keyser, J. 2000 Linear magnetohydrodynamic response of the magnetopause to magnetosheath fluctuations. *J. Geophys. Res.* **105**, 23 167–23 177.

Glassmeier, K. H., Mager, P. N. and Klimushkin, D. Y. 2003 Concerning ULF pulsations in Mercury's magnetosphere. *Geophys. Res. Lett.* **94**, 8276.

Klimushkin, D. Y., Leonovitch, A. S. and Mazur, V. A. 1995 On the propagation of transversally small-scale standing Alfvén waves in a three-dimensionally inhomogeneous magnetosphere. *J. Geophys. Res.* **100**, 9527–9534.

Lotko, W., Strelsov, A. V. and Carlson, C. W. 1998 Discrete auroral arc, electrostatic shock and suprathermal electrons powered by dispersive, anomalously resistive field line resonance. *Geophys. Res. Lett.* **25**, 4449.

Lu, J. Y., Rankin, R. Marchand, R. Tikhonchuk, V. T. and Wanliss, J. 2003 Finite element modeling of nonlinear dispersive field line resonances: trapped shear Alfvén waves inside field-aligned density structures. *J. Geophys. Res.* **108**, 1394.

Lui, A. T. Y. and Murphree, J. S. 1998 A substorm model with onset location tied to an auroral arc. *Geophys. Res. Lett.* **25**, 1269–1272.

Ofman, L. and Davila, J. M. 1996 Nonlinear excitation of global modes and heating in randomly driven coronal loops. *Astrophys. J. Lett.* **456**, L123.

Proehl, J. A., Lotko, W., Kouznetsov, I. and Geimer, S. D. 2002 Ultralow-frequency magnetohydrodynamics in boundary-constrained geomagnetic flux coordinates. *J. Geophys. Res.* **107**, 1225–1238.

Rankin, R., Samson, J. C. and Tikhonchuk, V. T. 1999 Discrete auroral arcs and nonlinear dispersive field line resonances. *Geophys. Res. Lett.* **26**, 663.

Rankin, R., Fenrich, F. and Tikhonchuk, V. T. 2000 Shear Alfvén waves on stretched magnetic field lines near midnight in Earth's magnetosphere. *Geophys. Res. Lett.* **27**, 3265–3268.

Salat, A. and Tataronis, J. A. 2000 Conditions for existence of orthogonal coordinate systems oriented by magnetic field lines. *J. Geophys. Res.* **105**, 13 055–13 062.

Singer, H. J., Southwood, D. J., Walker, R. J. and Kivelson, M. G. 1981 Alfvén wave resonances in a realistic magnetospheric magnetic field geometry. *J. Geophys. Res.* **86**, 4589.

Stern, D. P. 1970 Euler potentials. *Am. J. Phys.* **38**, 494–501.

Strelsov, A. V. and Lotko, W. 1999 Small scale 'electrostatic' auroral structures and Alfvén waves. *J. Geophys. Res.* **104**, 4411.

Takahashi, K., Denton, R. E., Anderson, R. R. and Hughes, W. J. 2004 Frequencies of standing Alfvén wave harmonics and their implication for plasma mass distribution along geomagnetic field lines: statistical analysis of CRRES data. *J. Geophys. Res.* **109**, 8202.

Walker, A. D. M., Ruohoniemi, J. M., Baker, K. B., Greenwald, R. A. and Samson, J. C. 1992 Spatial and temporal behavior of ULF pulsations observed by the Goose Bay HF radar. *J. Geophys. Res.* **97**, 12 187.

Warner, M. R. and Orr, D. 1979 Time of flight calculations for high-latitude geomagnetic pulsations. *Planet. Space Sci.* **27**, 679.

Waters, C. L. 2000 ULF resonance structure in the magnetosphere. *Adv. Space Res.* **25**, 1541–1558.